The 6th IASPEI / IAEE International Symposium: Effects of Surface Geology on Seismic Motion
August 2021

ESG6 BLIND PREDICTION. STEP1 BY INGV AND ENEA TEAM

Giuseppe Di Giulio[1], Salomon Hailemikael[2], Maurizio Vassallo[1] and Giuliano Milana[1]
1 Researcher, INGV Istituto Nazionale Geofisica e Vulcanologia, Rome, Italy (giuseppe.digiulio@ingv.it; maurizio.vassallo@ingv.it; giuliano.milana@ingv.it)
2 Researcher, ENEA Centro Ricerche Frascati, Rome, Italy (salomon.hailemikael@enea.it)

ABSTRACT

This paper describes the analysis performed within the ESG6 blind prediction step 1, devoted to the retrieval of the shear-wave velocity (Vs) structure at a target site in Kumamoto city. Ambient vibration data were analysed by different techniques. Horizontal-to-vertical spectral ratios were calculated showing resonance peaks around 0.3 and 1.1 Hz. Three methods were applied for surface-wave dispersion curve (DC) retrieval: cross-correlation (CC), modified spac (MSPAC) and high resolution F-K (RTBF). Vertical components were analysed to retrieve fundamental Rayleigh-wave DCs while horizontal motions allowed to extract Love-wave DC by RTBF. The Rayleigh-wave DCs from all methods are in good agreement. They were used as a target for numerical inversion jointly with Love-wave DC and Rayleigh-wave ellipticity curve obtained for one station. The retrieved Vs profiles are presented, and the comparison of our results with the best Vs model provided by the ESG6 committee is also discussed.

Keywords: ESG6, Kyoto, Japan, blind test step 1

INTRODUCTION

The determination of the Vs site profile is obtained in many seismological and engineering applications through recordings of ambient vibrations (i.e. seismic noise; hereinafter AMV) at the surface. Apart from the relative ease to collect seismic noise even in an urban environment, recent advances of both single-station and seismic array techniques (Bard et al. 2010) allow more accurate elaboration and estimation of both ellipticity and dispersion curve (DC). Indeed it is possible extracting the ellipticity of Rayleigh wave from field data discriminating the contribution of P-SV waves (Fäh et al. 2009; Hobiger et al. 2009), or to work with three-components (3C) signals to estimate also the DC of Love waves and the sense of particle motion of Rayleigh waves (Poggi and Fäh 2010; Maranò et al. 2017; Wathelet et al. 2018). New approaches based on the diffuse field assumption are also spreading (Kawase et al. 2015; Piña-Flores et al. 2016), along with the implementation of new inversion softwares based on it (Garcia-Jerez et al. 2016), or using the signed Rayleigh ellipticity (Wathelet et al. 2020). The step1 blind exercise gave us the opportunity to test our skill in AMV data analyses aimed at reconstructing velocity profiles. This exercise is based on the AMV data provided by ESG6 Committee through arrays with increasing aperture in the urban environment of Kumamoto district; this document shows the details and the results of our analysis.

DATA ANALYSIS

Brief data description

The data consists of 3-component ambient vibration data recorded by seismic sensors (eigen period 10 s) connected to high resolution data loggers (24 bits dynamic range) and deployed in 2-D array configuration. The 5 arrays (KUM-SS1, KUM-S, KUM-SM, KUM-M and KUM-LL) have nested triangular geometry (Fig. 1) with increasing aperture (larger side of the triangle ranging from about 2 m to 1200 m), therefore allowing for surface wave dispersion retrieval in a wide range of frequencies. Each array is made of 7 sensors. The ESG committee had also made available active seismic data that we decided to neglect for our analysis. The recording length is 45 minutes for KUM-SS1, 1 hour for KUM-S and 2 hours for the remaining arrays; recording sampling frequency is 200 Hz for all signals.

Recordings from the SS1 array were only used for single-station analysis. Due to a system malfunction in the NS component of one sensor, this channel data were discarded from the following analyses.

H/V Noise Spectral Ratios

The passive data were analyzed at first computing the horizontal-to-vertical (H/V) spectral ratios. We used the Geopsy code (Wathelet et al. 2020) using a running time-window of 120 seconds and a logarithmic smoothing algorithm (Konno and Ohmachi 1998). The H/V curves of all the arrays (KUM-SS1, KUM-S, KUM-SM, KUM-M and KUM-LL) consistently show two resonance peaks at about 0.3 and 1.1 Hz with amplitude as large as 4 and 8, respectively (Fig. 1). For the arrays with the largest aperture (KUM-SM, KUM-M and KUM-LL), the second resonance peak slightly increases in frequency up to 1.3 Hz. The systematic lower amplitude of the H/V curve calculated for station 01 is clearly visible from the comparison of the average H/V curves for the 3 lower aperture arrays and is due to the system malfunction of the NS component. Neglecting this outlier, the average curves are very similar and suggest that quite homogenous subsurface conditions may be assumed for the arrays. As expected, the average curves show larger dispersion (Fig. 1, middle panel) for the KUM-LL array, which spans a much wider area in which the unidimensional assumption may not strictly hold. However, also for KUM-LL H/V data the two frequency peaks are clearly observed.
The two resonance peaks are also shown by computing the H/V ratios as a function of the angle rotation in the horizontal plane (Fig. 2); we could not observe a clear polarization and we related the two peaks to the presence of seismic velocity contrasts along the depth profile.
H/V curve is considered as a proxy for the Rayleigh wave ellipticity (Fah et al. 2003), however the similarity of H/V and ellipticity is controlled by the relative proportion of Rayleigh waves and other seismic phases in the AMV wavefield. To extract the Rayleigh wave ellipticity curve to be used in surface wave inversion and evaluate the relative contribution of surface waves and body waves in the H/V composition, the Random Decrement Technique (Raydec; Hobiger et al. 2009) was applied to one station of KUM-S array. This method aims at suppressing the occurrence of seismic phases other than Rayleigh waves by stacking the narrow-band filtered time windows of the signals starting at positive zero-crossing of the vertical component of motion and projecting the corresponding horizontals into the direction which maximizes the correlation to the vertical with the theoretical 90° phase shift of the Rayleigh wave. Since the method applies to the 3-components of motion, station 1 was discarded due to the malfunction and station 7 was selected for the analysis. The Raydec ellipticity curve (Fig. 3) has a shape similar to the H/V curve calculated for the same station. The two curves have close amplitude above 2 Hz and show a main peak at 1.1 Hz. In terms of amplitudes, Raydec ellipticity shows lower values with respect to the corresponding H/V curve (maximum amplitude difference of 2.2 at 1.1 Hz). The Raydec curve stays below the H/V in the frequency range 0.4-2 Hz. The amplitude difference between the curves is almost constant (0.5) in the frequency range 0.4 Hz up to the first trough at 0.6 Hz. Finally Raydec ellipticity shows a lower frequency peak than H/V (below 0.3 Hz). This result suggests that whereas a significant uncertainty affects the low frequency resonance, the higher frequency resonance is well retrieved from both methods. In addition, the Rayleigh wave predominance in the ambient vibration wavefield seems confirmed for the higher frequency range (above 2 Hz) where the curves are closer, whereas the relative contribution of the other different phases increases and varies with frequency in the lower range.

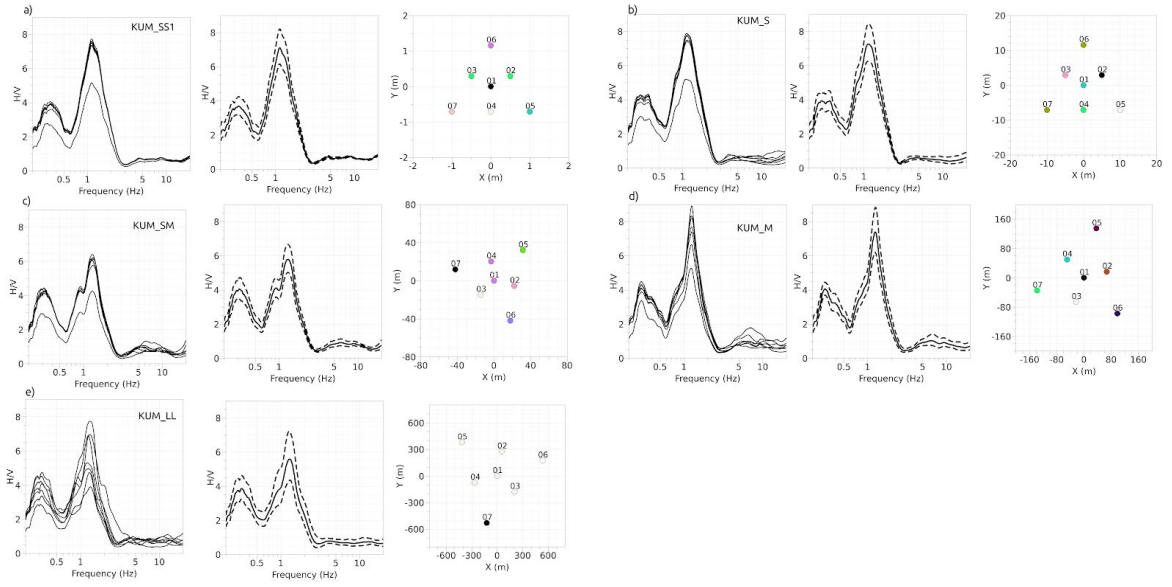

Figure 1. H/V curves at the five arrays with increasing aperture: KUM_SS1 (a), KUM_S (b), KUM_SM (c), KUM_M (d) and KUM_LL (e). The average H/V curves at the seven stations, their mean curve with standard deviation, and array geometry are also shown from left to right in each panel.

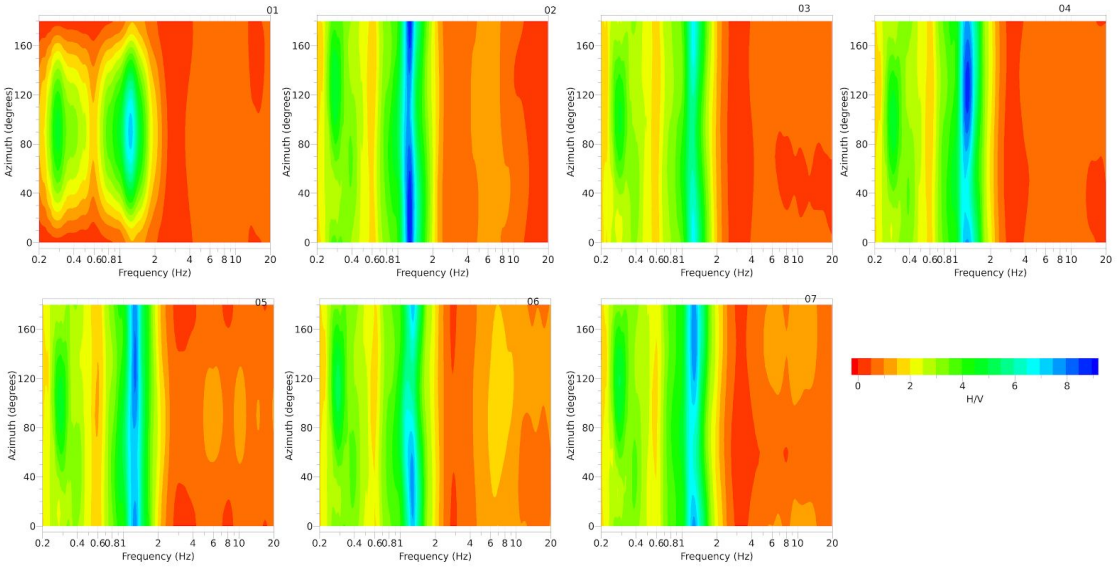

Figure 2. H/V amplitude distribution in the horizontal plane as a function of the azimuth at the KUM_M array (the station 01 is not working properly). The scale color is proportional to the amplitude of the H/V curves.

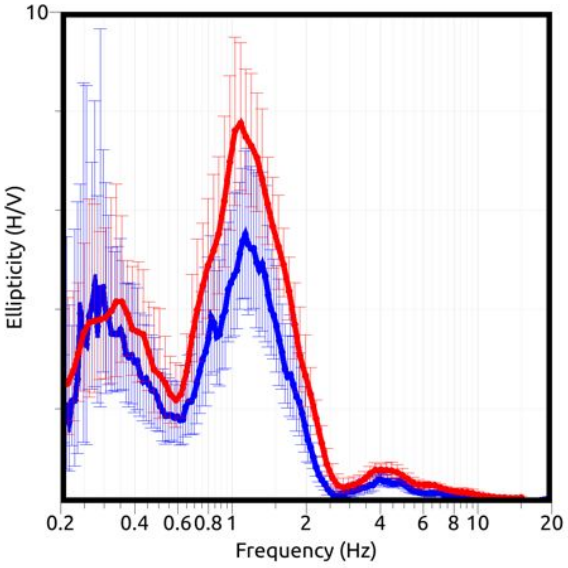

Figure 3. Station #7 of the KUM_S array. Comparison between the H/V curve (in red) and the ellipticity curve (in blue) after the RayDec analysis (Hobiger et al. 2009).

Cross-Correlation analysis

The Cross-Correlation (CC) method was also applied to the vertical components using an *ad hoc* software. To this aim, for each array, the synchronized recordings of vertical components are processed using one-bit normalization and spectral whitening (Bensen et al. 2007). Then, the cross-correlation functions are computed for the processed traces at the different station pairs of arrays.

To compute the dispersion curve of the seismic signals emerging from the cross-correlation functions, we applied a velocity analysis to the CCs functions. The used method is similar to the Constant Velocity Stack (CVS) analysis (Yilmaz, 1987), very popular in active seismic reflection processing and already used in different Italian areas (Vassallo et. al. 2019, Di Giulio et al. 2020). The cross-correlation functions were filtered in different frequency bands starting from 0.5 to 20 Hz. For each band, the cross-correlation functions were shifted back in time according to the theoretical surface travel times computed for different constant velocities starting from 50 m/s until 2000 m/s using a velocity step of 10 m/s. For each frequency band and applied velocity correction, the Phase-Weighted Stack (PWS, Schimmel and Paulssen, 1997) is computed, and the absolute maximum of PWS is used to estimate the presence of a horizontally aligned phase in the corrected seismic section. For each filter, the maximum of stack function provides the velocity of surface waves at the considered frequency.

Fig. 4 shows the computed cross-correlations functions (organized according to the distance between station pairs) and the related results of velocity analysis performed for the different arrays. For each array, the dispersion curve (black line) is identified on the basis of the maximum value of the stack function at each frequency and exploiting the lateral continuity of the maximum values in the investigated frequency range. Fig. 5 shows the dispersion curves derived from each array and the dispersion curve obtained by joining the different segments from the individual arrays in the frequency band 1-20 Hz.

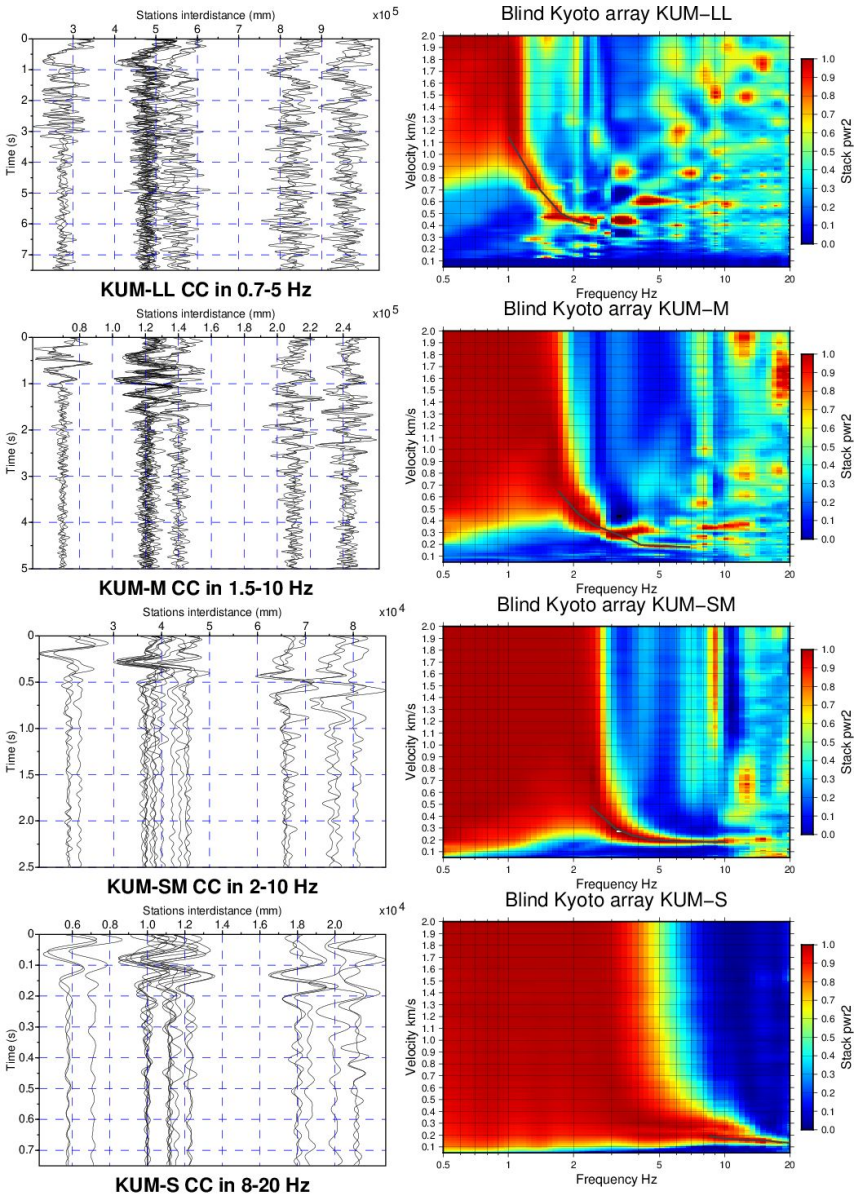

Figure 4. The figures on the left show the cross-correlation functions for the different arrays. Only to improve the clarity of each figure, the CCs are filtered in different frequency ranges depending on the array. The results of the performed velocity analysis with the relative dispersion curve identified (black lines) are on the right.

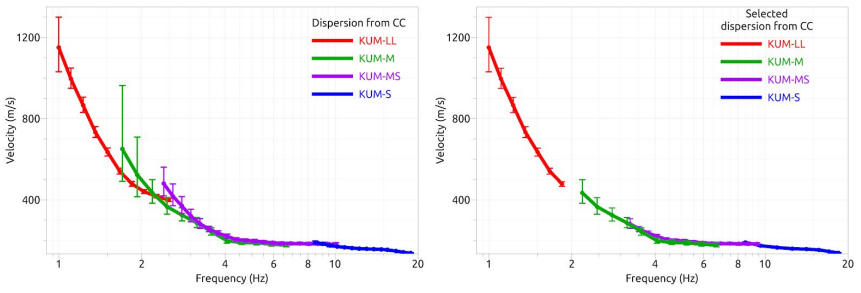

Figure 5. The left panel shows the dispersion curves derived from Cross-Correlation analysis of the different arrays. The right panel shows the selected dispersion curve.

MSPAC analysis

The spatial autocorrelation method (SPAC) is based on Aki work (Aki 1957) which is intended for arrays with semi-circular geometry and fixed radius. This approach was implemented for irregular geometries (MSPAC) by Bettig et al. (2001); we performed such analysis using the Geopsy software (Wathelet et al 2020). The Rayleigh wave dispersion curve was estimated by fitting the SPAC coefficients to the first-order Bessel function assuming that the microtremors are mainly composed of fundamental-mode Rayleigh waves and assuming stationarity of the AMV wavefield generated by a spatially homogeneous distribution of sources. Several studies demonstrated that this assumption is more easily fulfilled by using long duration records and with sources widely distributed in azimuth. In this way it's possible to stabilize the evaluated zero lag correlation function and better estimate the average statistical properties of the AMV wavefield (Aki 1957; Okada 2006). The obtained Rayleigh wave DC is given by combining the estimates for the different arrays which provide resolution in different frequency bands: in the range 0.6-1.2 Hz for KUM-LL, in the range 1.8-2.2 Hz for KUM-M, in the range 2.5-3.2 Hz for KUM-S and between 3.5 and 9 Hz for KUM-SS1 (Fig. 6). Phase velocities are roughly constant, 200 m/s, between 9 and 4 Hz; in the lower frequency range phase velocities steadily increase from this value up to 1400 m/s at 1 Hz (Fig. 6). At lower frequencies, the estimated DC flattens between 0.7 and 1 Hz and suddenly increases again up to velocity of 1900 m/s at 0.6 Hz.

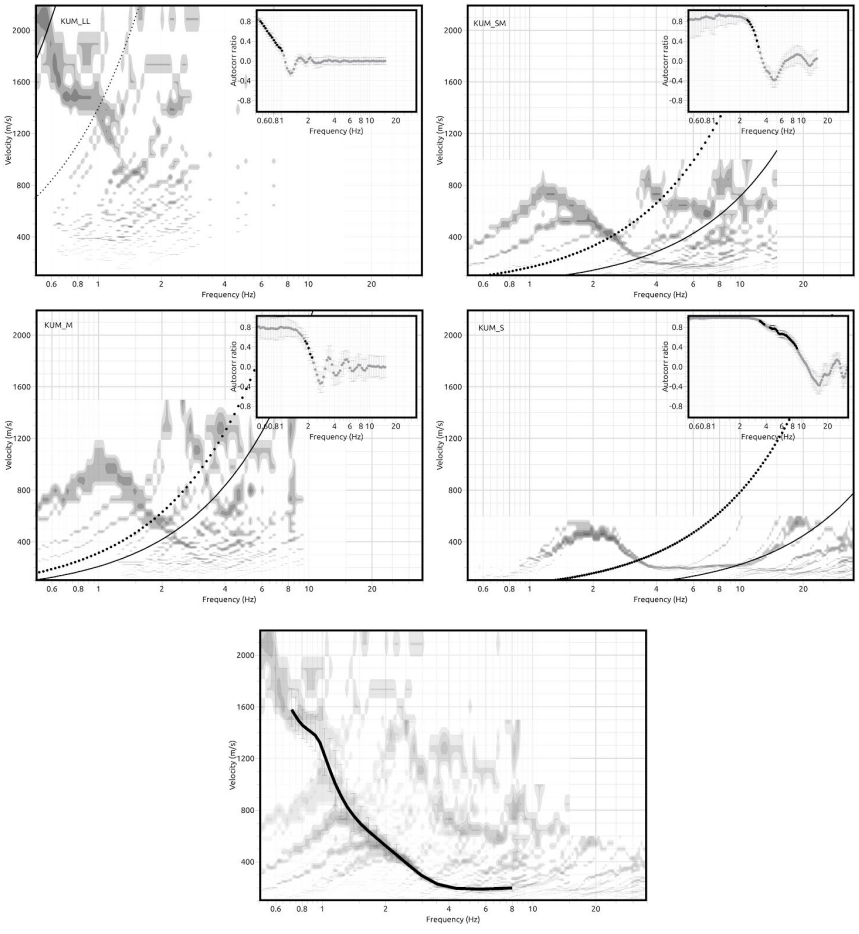

Figure 6. MSPAC estimate of phase velocities as a function of frequency including resolution limits for the different arrays (top and middle panels). Estimated azimuthal averaged autocorrelation ratios as a function of frequency for one ring of the coarray associated to the respective triangular seismic array (insets in top and middle panels). In the bottom panel the picking of the final wideband Rayleigh-wave dispersion curve is shown.

Three-components RTBF analysis

We used the passive signals of the three largest arrays: KUM-LL, M and SM. We derived Rayleigh and Love phase dispersion curves (Fig. 7) searching from the FK maxima in the wavenumber plane (kx, ky) using the Geopsy tool. The frequency range of analysis for each selected array was based on the resolution and alias limits (Wathelet et al., 2008). The results of the three arrays (Fig. 7) are in good agreement both for Rayleigh and Love DCs within the frequency band from 0.7 up to 4 Hz. The Love DC shows lower velocities except at around 4 Hz, where the Rayleigh and Love share the same values of phase-velocity.

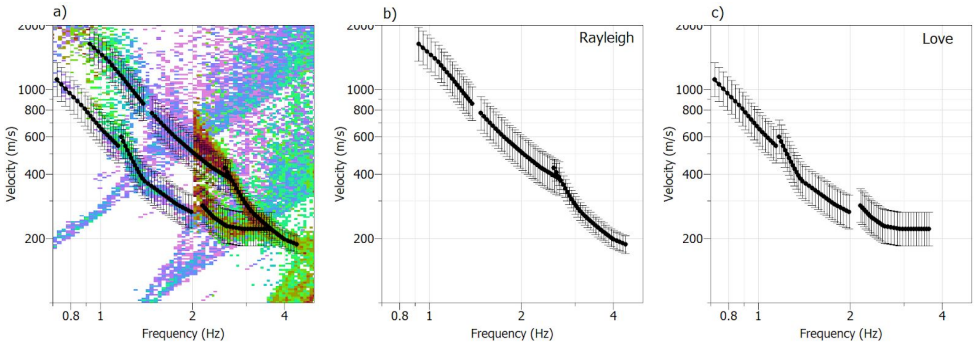

Figure 7. Rayleigh and Love DCs estimated from RTBF analysis. Results are overlaying in a) for the KUM_LL, KUM_M and KUM_SM arrays. The color scale is proportional to normalized probability density. The DCs are also shown separately in b) and c), respectively.

DCs COMPARISON AND TARGET DISPERSION CURVE SELECTION

DCs obtained from the different methods show a very good agreement (Fig. 8), and allow to select a combined Rayleigh curve in a wide frequency band (from 0.71 to 20 Hz). The Rayleigh DC obtained by the three methods are all included within their experimental uncertainty in the frequency range 1.5-8 Hz. The most significant discrepancy in the DCs is observed in the lowest frequencies part (i.e. 0.7-1 Hz) where RTBF analysis gives higher phase-velocities with respect to MSPAC analysis (Fig. 8d). We decided to select at the lowest frequencies the MSPAC curve, because the spatial autocorrelation method in principle can provide a better resolution (Ohori et al. 2002) assuming the plane-wave stationarity and an isotropic AMV wavefield. Table 1 explains how the target DCs were selected, with the indication of the method of analysis and of the frequency band. The target Rayleigh DC was selected combining the MSPAC results below 1 Hz (using data from KUM_LL to KUM_S arrays), the CC results above 8 Hz and averaging the DCs obtained from the three methods in the range 1.5-8 Hz. The RTBF analysis has provided the Love DC in the range 0.74-3.5 Hz.

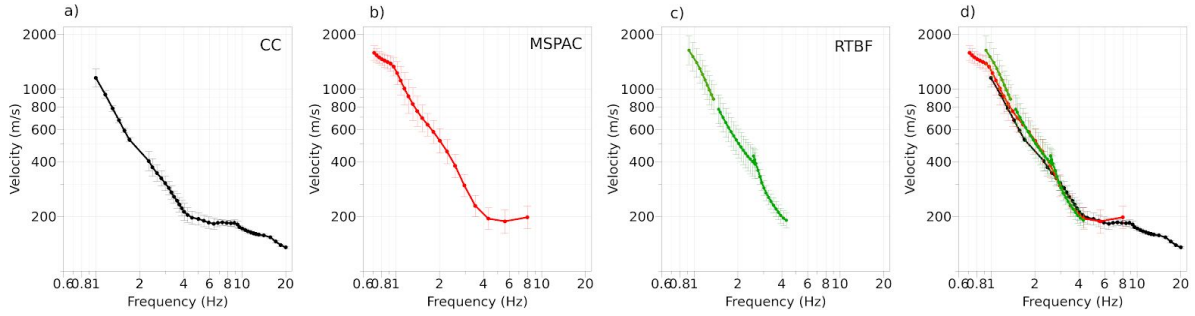

Figure 8. Rayleigh-wave DC estimated using CrossCorrelation (a), MSPAC (b) and RTBF analysis (c). The DCs are overlaid in (d).

Table 1. Frequency range limits of DCs.

array name	CC (used for Rayleigh dc) frequency band (Hz)	MSPAC (used for Rayleigh dc) frequency band (Hz)	RTBF (used for Love dc) frequency band (Hz)
KUM_SS1 (not used)			
KUM_S	9.6-20	3.5-9.0	
KUM_SM	8-9	2.5-3.2	2.5-3.5
KUM_M		1.8-2.2	1.3-2
KUM_LL		0.7-1.2	0.74-1.1

JOINT INVERSION OF DCs AND ELLIPTICITY

Rayleigh and Love dispersion curves were jointly inverted using the Geopsy tool for deriving an S-wave velocity profile through an improved neighborhood algorithm (Wathelet et al., 2008). The model space was defined by several layers based on the JIVSM and Chimoto et al. (2016) models. We tested different model parameterization during the inversion, and the most convincing models, obtained using seven layers overlaying a seismic bedrock (Table 2), are shown in Figure 9. S-wave velocities within the model space parameterization were allowed to vary in a range of +/- 50% with respect to the available values in these models. A linear increase of S-wave velocity with depth was allowed for the uppermost layer (maximum thickness of 25 m; see Table 2). Density in each layer was fixed considering the cited models.

We also used as additional constraint the fundamental mode Rayleigh-wave ellipticity as derived by Raydec analysis (Fig. 3) at the S array (station no. 7). Although Geopsy allows taking into account for the sign of ellipticity (i.e. prograde or retrograde), we preferred using the absolute value of the Rayleigh ellipticity. During the inversion, we tried to fit the two ellipticity peaks (at about 0.3 Hz and 1 Hz) and the main trough (at about 3 Hz) present in the retrieved Rayleigh-wave ellipticity curve (fundamental mode). Overall, we obtained a good fit between our results and the observations (Fig. 9). The results are shown for a misfit value lower than 0.4 (misfit is representative of the deviation between models and experimental curves). The absence of a frequency gap between the DC and ellipticity curves improves the stability of the inversion results. The best fit model (misfit = 0.36) shows shallow velocities ranging from 150 to 250 m/s in the top 20 m. Vs increases up to 400 m/s down to 80 m depth, where a first Vs discontinuity is found and the velocity reaches a value of about 1000 m/s. This Vs value extends down to roughly 400 m depth, where a second Vs sudden increase to 1700 m/s is observed. The main seismic impedance contrast is estimated at a large depth around 1500 m, where the seismic bedrock Vs is estimated to be larger than 3700 m/s. It is worth noting that the bedrock depth estimate is mainly controlled by the low-frequency peak in the ellipticity curve.

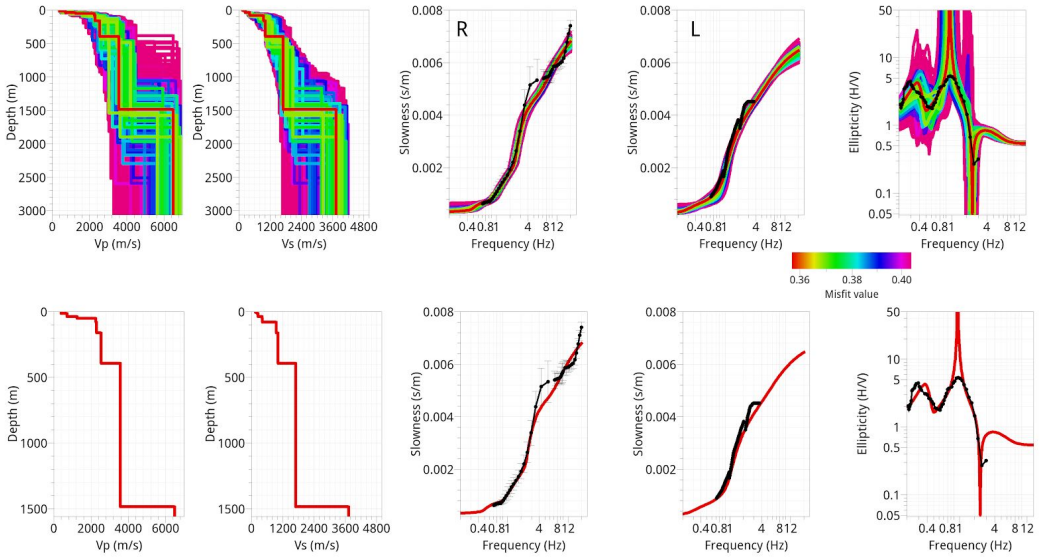

Figure 9. From Left to the Right) Vp and Vs models derived from the joint inversion of Rayleigh (R) and Love (L) DC (fundamental mode), and with the absolute Rayleigh-wave ellipticity. The experimental curves are plotted in black, whereas the models are plotted in a rainbow scale proportional to the misfit obtained during the inversion. The best model (i.e. minimum misfit) is shown in the bottom panel.

Table 2. Model parameterization used in the inversion shown in Figure 9.

Layer #	Velocity-depth relation	Vp range [m/s]	Vs range [m/s]	Density [Kg/m^3] (fixed)	Poisson ratio	Thickness range [m]
1	linear increase for Vs uniform for Vp	140-420	from 80-200 to 100-250	1600	0.2-0.5	1-25
2	uniform	430-1300	250-750	1800	0.2-0.5	1-25
3	uniform	900-2000	350-750	1950	0.2-0.5	5-215
4	uniform	1500-2500	800-1200	2070	0.2-0.5	10-400
5	uniform	1500-3000	650-2000	2200	0.2-0.5	10-200
6	uniform	1500-4000	1000-3000	2350	0.2-0.5	20-800
7	uniform	2500-4500	1200-3600	2450	0.2-0.5	50-2000
Half-space		2500-6900	1600-4800	2700		

DISCUSSION AND CONCLUSIONS

This blind test was useful to verify the reliability of the strategy usually adopted by the authors in the analysis of seismic noise. AMV data provided by ESG6 committee are characterized by a significant contribution of surface waves, and the use of arrays with increasing aperture allows to derive a

dispersion in a wide frequency range (from 0.7 to 20 Hz). Moreover the geometry composed of two nested triangles using seven seismic stations, which was never tested by the authors, proved very convenient since it allows the deployment in the field of good azimuthal coverage with a limited number of sensors. We have adopted different techniques of analysis obtaining very consistent results in terms of Rayleigh-wave dispersion (Fig. 8d). Further, the Raydec and RTBF analyses allow to extract Rayleigh-wave ellipticity and the Love-wave dispersion, respectively. The best fit model derived from the joint inversion is shown in Fig. 9. A good agreement between experimental and theoretical curves is observed, except in the frequency band 4-6 Hz where the theoretical Rayleigh DC is not able to follow the inflection of the experimental DC. After the blind test step 1, the ESG6 Committee has made available its preferred model for the target site. We compared this model with our results in Fig. 10, finding a satisfactory agreement between the two. The first 400 m of the velocity profiles are very similar, and also the deep seismic contrast around a depth of 1500 m is matched by both models. The main difference is in the depth of the intermediate seismic velocity contrast, 400 m by our model versus 600 m by ESG6 model. On average, our model shows lower Vs values between 400 and 1500 m, and some discrepancies are also observed in the density values (which were fixed during our inversion). The comparison between the two models is also performed in terms of SH transfer functions (Fig. 11) computed by the reflectivity method (Kenneth and Kerry, 1979), showing a general agreement with some differences in the amplification values, mainly in the lower frequency range (i.e. < 1 Hz) and between 1.5 and 2 Hz.

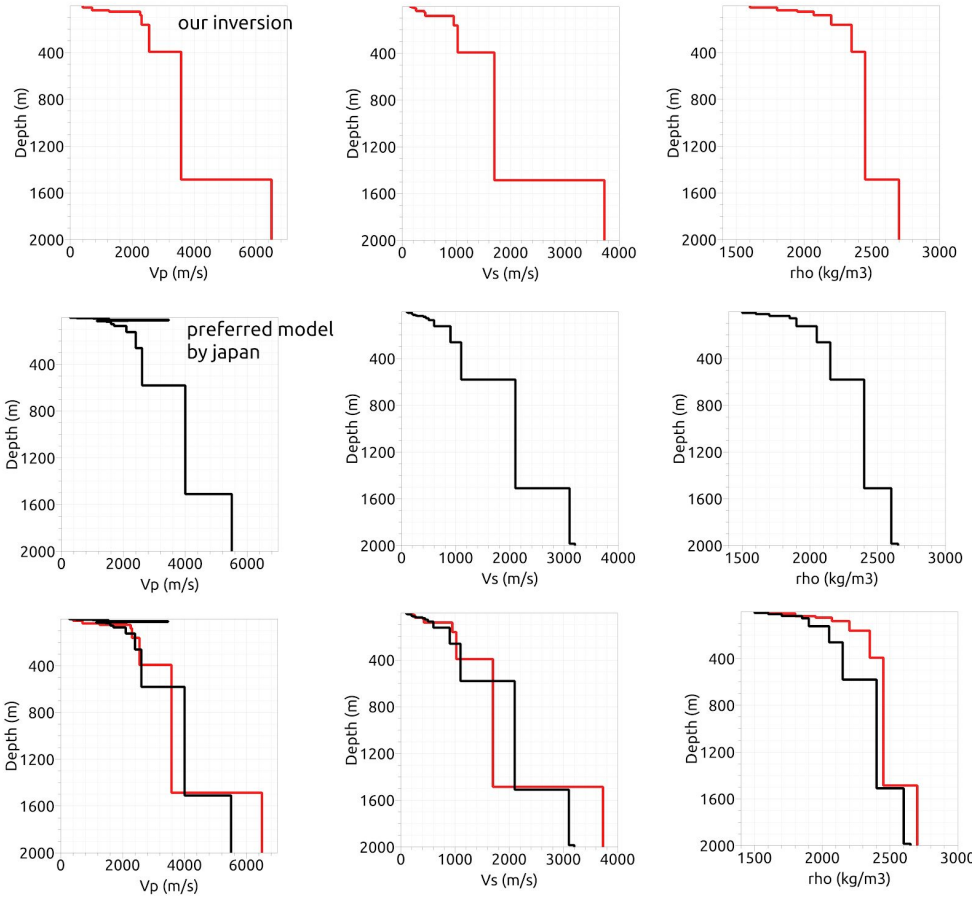

Figure 10. Comparison between our best model (in red) derived from the joint inversion and the preferred ESG6 model (in black). The density values in our inversion were fixed.

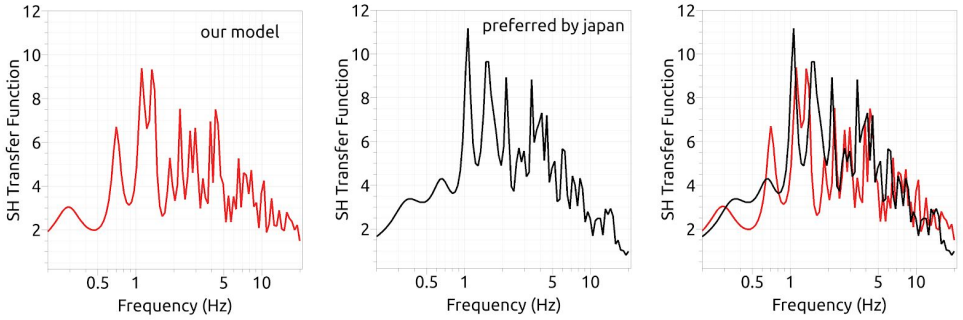

Figure 11. SH transfer functions computed by means of the gpsh tool (Qp and Qs values were set equal to 1/10 of Vp and Vs values, respectively). Comparison between our best model (in red) derived from the joint inversion and the preferred ESG6 model (in black).

REFERENCES

Aki, K., (1957). "Space and time spectra of stationary stochastic waves, with special reference to microtremors", *Bull. Earthq. Res. Inst.*, **35**, 415–457.

Bard, P.Y., Cadet, H., Endrun, B., Hobiger, M., Renalier, F., Theodulidis, N., Ohrnberger, M., Fäh, D., Sabetta, F., Teves-Costa, P. and Duval, A.M. (2010). "From non-invasive site characterization to site amplification: recent advances in the use of ambient vibration measurements", In *Earthquake Engineering in Europe* (pp. 105-123). Springer, Dordrecht.

Bensen, G.D., Ritzwoller, M.H., Barmin, M.P., Levshin, A.L., Lin, F., Moschetti, M.P., Shapiro, N.M. and Yang, Y., (2007). "Processing seismic ambient noise data to obtain reliable broad-band surface wave dispersion measurements". Geophysical journal international, **169**(3), pp.1239-1260.

Bettig, B., et al. (2001). "Analysis of dense array noise measurements using the modified spatial auto-correlation method (SPAC): application to the Grenoble area", *Bollettino di Geofisica Teorica ed Applicata*, **42**(3-4), pp.281-304.

Chimoto, K., et al. (2016). "Estimation of shallow S-wave velocity structure using microtremor array exploration at temporary strong motion observation stations for aftershocks of the 2016 Kumamoto earthquake", *Earth Planets Space,* **68**(206), doi:10.1186/s40623-016-0581-3.

Di Giulio, G., Ercoli, M., Vassallo, M. and Porreca, M., (2020). "Investigation of the Norcia basin (Central Italy) through ambient vibration measurements and geological surveys". *Engineering Geology*, **267**, p.105501.

Fäh, D., Wathelet, M., Kristekova, M., Havenith, H., Endrun, B., Stamm, G., Poggi, V., Burjanek, J. and Cornou, C., (2009). "Using ellipticity information for site characterisation", *NERIES JRA4 Geotechnical Site Characterisation, task B 2*.

García-Jerez, A., Piña-Flores, J., Sánchez-Sesma, F.J., Luzón, F. and Perton, M., (2016). "A computer code for forward calculation and inversion of the H/V spectral ratio under the diffuse field assumption", *Computers & Geosciences*, **97**, pp.67-78.

Hobiger, M., Bard, P.Y., Cornou, C. and Le Bihan, N., 2009. (2009). "Single station determination of Rayleigh wave ellipticity by using the random decrement technique (RayDec)", *Geophysical Research Letters*, **36**(14).

Kawase, H., Matsushima, S., Satoh, T. and Sánchez-Sesma, F.J., (2015). "Applicability of theoretical horizontal-to-vertical ratio of microtremors based on the diffuse field concept to previously observed data", *Bulletin of the Seismological Society of America*, **105**(6), pp.3092-3103.

Kennett, B. L. and N. J. Kerry (1979). "Seismic waves in stratified half space", *Geophys. J. R. Astron. Soc.,* **57**, 557-583.

Konno, K. and Ohmachi, T., (1998). "Ground-motion characteristics estimated from spectral ratio between horizontal and vertical components of microtremor", *Bulletin of the Seismological Society of America*, **88**(1), pp.228-241.

Maranò, S., Hobiger, M. and Fäh, D., (2017). "Retrieval of Rayleigh wave ellipticity from ambient vibration recordings", *Geophysical Journal International*, **209**(1), pp.334-352.

Ohori, M., Nobata, A., & Wakamatsu, K. (2002). "A comparison of ESAC and FK methods of estimating phase velocity using arbitrarily shaped microtremor analysis", *Bulletin of the Seismological Society of America*, **9**2, 2323–2332.

Okada, H., (2006). "Theory of efficient array observations of microtremors with special reference to the SPAC method", *Exploration Geophysics*, **37**(1), pp.73-85.

Piña-Flores, J., Perton, M., García-Jerez, A., Carmona, E., Luzón, F., Molina-Villegas, J.C. and Sánchez-Sesma, F.J., (2016). "The inversion of spectral ratio H/V in a layered system using the diffuse field assumption (DFA)", *Geophysical Journal International*, **208**(1), p. 577–588, https://doi.org/10.1093/gji/ggw416

Poggi, V. and Fäh, D., (2010). "Estimating Rayleigh wave particle motion from three-component array analysis of ambient vibrations", *Geophysical Journal International*, **180**(1), pp.251-267.

Schimmel, M. and Paulssen, H., (1997). "Noise reduction and detection of weak, coherent signals through phase-weighted stacks". *Geophysical Journal International*, **130**(2), pp.497-505.

Vassallo, M., De Matteis, R., Bobbio, A., Di Giulio, G., Adinolfi, G.M., Cantore, L., Cogliano, R., Fodarella, A., Maresca, R., Pucillo, S. and Riccio, G.(2019). "Seismic noise cross-correlation in the urban area of Benevento city (Southern Italy)", *Geophysical Journal international*, **217**(3), pp.1524-1542.

Wathelet, M., D. Jongmans, M. Ohrnberger, and S. Bonnefoy-Claudet (2008). "Array performances for ambient vibrations on a shallow structure and consequences over Vs inversion", *J. Seismol.,* **12**, no. 1, 1–19.

Wathelet, M., Guillier, B., Roux, P., Cornou, C. and Ohrnberger, M., (2018). "Rayleigh wave three-component beamforming: signed ellipticity assessment from high-resolution frequency-wavenumber processing of ambient vibration arrays", *Geophysical Journal international*, **215**(1), pp.507-523.

Wathelet, M., Chatelain, J.L., Cornou, C., Giulio, G.D., Guillier, B., Ohrnberger, M. and Savvaidis, A., (2020). "Geopsy: A User‐Friendly Open‐Source Tool Set for Ambient Vibration Processing", *Seismological Research Letters*, **91**(3), pp.1878-1889.

Yilmaz O. (1987). "Seismic data processing in Investigations" in *Geophysics, 2: Soc. Expl. Geophys,* series Eds., eds Doherty S.M., Neitzel E.B.